Simulation and Experimental Study on Rock-Breaking Mechanism of the Reverse Rotary Torque Self-balancing Dual Drill Bit

Simulation and experimental study on rock-breaking mechanism of the reverse rotary torque self-balancing dual drill bit

Cong Zhang [a,b,c], Ke Gao [a,b,c], Yan Zhao [a,b,c*], Xiaobo Xie [a,b,c], Congshan Zhang[a,b,c], Xiaoshu Lv [a,d,e]

a College of Construction Engineering, Jilin University, Changchun, Jilin, 130026, China

b Engineering Research Center of Geothermal Resources Development Technology and Equipment, Ministry of Education, Jilin University, Changchun, 130026, China

c Key Laboratory of Drilling and Exploration Technology in Complex Conditions of Ministry of Natural Resources, Jilin University, Changchun, Jilin, 130026, China

d Department of Electrical Engineering and Energy Technology, University of Vaasa, P.O.Box 700, FIN-65101, Vaasa, Finland

e Department of Civil Engineering, Aalto University, P.O.Box 12100, FIN-02130, Espoo, Finland

Abstract: The stick-slip vibration of a drill bit in oil and gas drilling causes significant disturbances to the formation, severely impacting the drilling quality. The dual drill bit (DB) torque self-balancing drilling technology has superior drill bit stability, obtained by balancing the torques of the inner and outer bits (IB and OB). However, research on the DB working process is still in the initial stages. To analyze the vibration reduction of the DB from the perspective of the rock-breaking mechanism, this study established a dynamic rock-breaking finite element model of the DB through theoretical calculations, and conducted a numerical simulation comparison and drilling experiment comparison of the rock-breaking process between the DB and conventional drill bit (CB). The differences in the reactive torque between the DB and CB were compared. Subsequently, the drilling process was simulated using the two drilling methods, including the rock-breaking process, core and wellbore disturbance, and bit motion. The results indicate that DB drilling can reduce the torque vibration of the rock on the drill bit by 69.7%, thus decreasing the damage to the formation. In addition, DB can form a shear breaking effect on the rock at the junction of IB and OB, which improves the rock-breaking efficiency by 13.8%. The results of this work will help reveal the low stick-slip vibration mechanism of the DB self-balancing drilling technique, which can provide new ideas for the study of drilling stability.

Keywords: Torque self-balancing dual drill bit; Rock-breaking mechanism; Stick-slip vibration; Drilling stability

List of symbols

p	Load distribution of the diamond particle (pa)
p_0	Pressure at the center of circle (pa)
r	Distance from any point in the stress region to the center of the circle (m)
a	Radius of a diamond particle (m)
n	Stress distribution index (dimensionless)
F_n	Normal contact pressure between diamond particle and rock (N)
F_t	Shear force at the center of circle (N)
M	Torque applied to the bit ($N \cdot m$)
k	Number of diamond particles per element area (dimensionless)
F_T	Force per element area consumed in rock breaking and friction (N)
l	Radius of integral micro element (m)
R_a	Inner diameter of the bit (m)

R_b	Outer diameter of the bit (m)
M_s	Reactive torque of the CB ($N \cdot m$)
M_i	Reactive torque of the IB ($N \cdot m$)
M_o	Reactive torque of the OB ($N \cdot m$)
M_d	Combined reactive torque of the DB ($N \cdot m$)
N	Weight on bit (N)
T	Toque of bit ($N \cdot m$))
S	Bit area (mm^2)
ω	Bit rotating speed (rpm)
v	Rate of penetration (mm/s)

1 Introduction

Depletion of shallow resources has led to an increase in drilling depth requirements, and borehole structures have become increasingly complex [1]. The structure and mechanical properties of the formation will change owing to changes in ground stress, as evidenced by an increase in rock strength and a decrease in formation drillability, which in turn affects the efficiency of the drill bit in breaking rock [2]. Meanwhile, as the length of the drilling string increases, the movement of the downhole drill bit becomes more complex [3].

The vibration of the drill bit under a rotary drilling process disturbs the wellbore and core, which greatly affects the drilling efficiency and quality [4]. As the weight on the bit and rotation speed increase, the bit vibration intensifies. However, an increase in the height and width of the rock ridge will facilitate the stability of the bit [5]. During the drilling of the gas-hydrate-bearing stratum, the pressure core sampler bit also disturbed the undrilled sub-bottom hole near the cutting shoes and underground layer around the well near the bit, which made it difficult to obtain accurate information on the gas hydrate formation by core drilling analysis and logging [6]. The torque variation of the bit was particularly significant when drilling complex formations including soft-hard interbedded rock. Under these severe conditions, bit cutters are easily crushed and broken [7]. When sliding drilling with curved housing drilling fluid motors, the reactive torque generated by the bit is too high, which significantly affects the guiding effect [8]. In horizontal well drilling, as the driven torque aggregates and releases, the drill string acts as a low-side local stick-slip and tumbling motion, which causes damage to the drill string and wellbore [9]. The back-torsional oscillation of the drilling string is largely caused by stick-slip vibration, and reducing it helps reduce the disturbance to the formation and core at the bottom hole.

Stick-slip motion is a dynamically unstable vibration caused by the transition between static and kinetic frictions [10]. The periodic accumulation and release of energy in the drill string when the bit overcomes the frictional torque at the bottom of the borehole can easily cause stick-slip vibration, which not only accelerates the wear of the bit, but also intensifies the disturbance of the surrounding formation and core [11]. Numerous studies have attempted to attenuate this negative state. Kyllingstad et al. [12] developed a simple pendulum model to study the stick-slip vibration of a drill string, and suggested that the stick-slip vibration could be effectively suppressed by reducing the weight on bit (WOB) or decreasing the rotary speed. Besselink et al. [13] stated that the stick-slip vibration on a bit could be suppressed by optimizing its axial vibration. Liu et al. [14] used the optimal feedback gain method to control the stick-slip vibration of a nonlinear drilling string system and achieved certain control effects. Zhu et al. [15] indicated that high-frequency torsional shock can effectively suppress stick-slip vibration. Tian et al. [16] studied the influence of the PDC bit cutter layout on the stick-slip vibrations of deep drilling systems. Previous studies have mainly adopted optimizing the drilling tool combination configuration, drilling parameters, or control method to attenuate stick-slip vibration. The root cause, however, is that most existing drilling technologies use a drill string to deliver torque over long

distances. The result of the growth of the drill string is a reduction in its equivalent torsional stiffness, followed by severe losses, poor controllability, and low efficiency. The torque transmitted to the bit is discontinuous and variable, which in turn causes stick-slip vibration of the drill string.

In order to reduce the stick-slip vibration of drill bit, Gao et al. [17] proposed a *downhole drilling tool system of torque self-balancing*. As shown in Fig. 1, the principle is to drive a simultaneous reverse rotation of the dual drill bit (DB), consisting of an inner drill bit (IB) and an outer drill bit (OB), using downhole power components. The pressure adjustment system is used to adjust the weight on the IB and OB, which creates a mutual balance of the torque downhole, thus counteracting the reactive torque generated by the rotation of the drill string during conventional drilling. This drilling method ensures the stable operation of the downhole drilling tools, which is conducive to weakening the wellbore instability caused by stick-slip vibration.

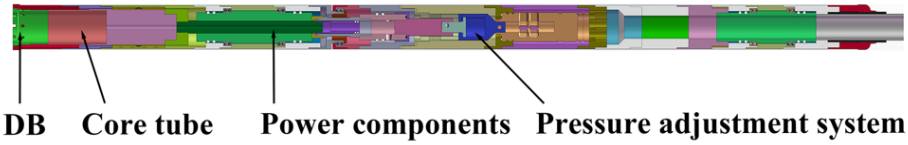

Fig. 1. Schematic of the downhole drilling tool system of torque self-balancing [18]

Some scholars have studied the mechanism of rock-breaking using DB. Gao et al. [19] established a rock-breaking model of DB and analyzed the force state of the bit and rock during the rock-breaking process of the conventional bit (CB) and DB using the ANSYS/LS-DYNA software. It was concluded that DB drilling produced more stress concentration points and higher stress values on the rock at the bottom of the well compared with CB drilling, which was conducive to improving the rock-breaking efficiency. However, it lacked disturbance analysis of the wellbore and core, as well as vibration analysis of the drill bit. In addition, the bottom surface of the bit model used in the simulation was flat, which is a common deficiency in diamond-bit drilling simulations [20]. Therefore, further and more accurate research is required on the mechanism of micro-disturbance rock-breaking with DB. With the development of computer technology, the use of computer simulation technology to study the rock-breaking mechanism of drill bits has gradually become a convenient and feasible research method, mainly including the discrete element method (DEM) and finite element method (FEM). Rojek et al. [21] used DEM to conduct a simulation study on the process of rock breaking using a drill bit. The results showed that the DEM can model the bit-breaking rock quantitatively and obtain an average cutting force in good agreement with the laboratory results. Zhu et al. [22] compared and analyzed the macro and micro characteristics of attapulgite broken using bionic and conventional cutting tools based on the DEM software. A high crushing efficiency of the bionic cutter for crushing attapulgite was obtained. Jaime et al. [23] concluded that rock cutting could be reasonably modeled using a plasticity-damage model based on the FEM, an element erosion scheme that removes an element when its energy release equals fracture energy.

In summary, CB is prone to large stick-slip vibrations during drilling, which has a limited rock-breaking efficiency. DB is superior in improving the stability of the drill bit. However, few studies have analyzed vibration reduction from the perspective of the rock-breaking mechanism. In this study, taking granite as the research object, two types of drill bits were established using FEM, and rock-breaking simulations were performed. Subsequently, the differences in the rock-breaking mechanism, wellbore and core disturbance, and bit motion between the DB and CB were compared. Finally, the simulation results were verified through drilling experiments. This study is expected to provide a new perspective for reducing the vibration of drill bits.

2 Nonlinear dynamics model

2.1 Damage model of the rock

Both conventional and dual diamond drill bits rely on exposed diamond particles to break rocks. The working process of a single-grain diamond is equivalent to the contact between a rigid sphere and rock, for which we performed a force analysis. As shown in Fig. 2, the diamond particle first crinkles and crushes the rock under normal pressure and then carves the rock under tangential shear [24]. Fracture damage chips are generated at the front of the diamond particle, whereas spalling chips are at the back. Therefore, the force analysis of diamond particles in breaking rocks must be considered from both normal and tangential load distributions [25].

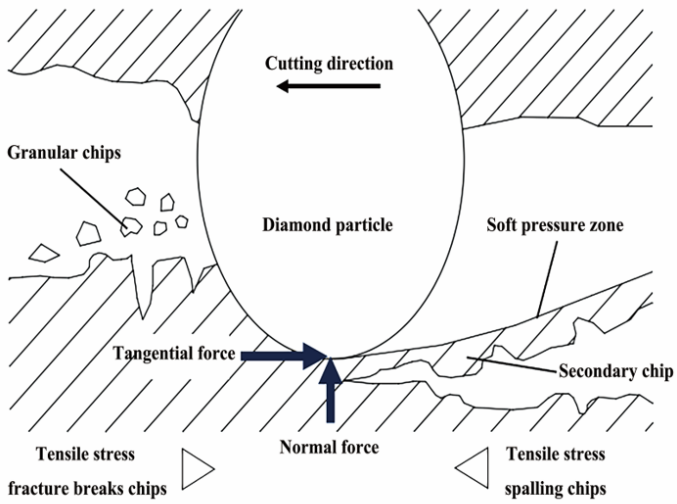

Fig. 2. Schematic of the rock broken by a diamond particle [26]

The Hertz contact theory provides a calculation method for the contact force between a rigid sphere and elastic half-space body [27]. As the hardness of diamond is far greater than that of rock, it is regarded as a rigid sphere. By applying a circular normal distributed load to the surface of an elastic half-space body, the contact stress becomes non-linear with the applied pressure [28]. The expression for the load distribution is:

$$\mathrm{p} = p_0(1-\frac{r^2}{a^2})^n \tag{1}$$

where p_0 is the pressure at the center of the circle, r is the distance from any point in the stress region to the center of the circle, n is the stress distribution index, and a is the radius of the diamond particle. As the load was spherically distributed, n was set to $\frac{1}{2}$.

The normal contact pressure between diamond particle and rock can be calculated as

$$F_n = \int_0^a p_0(1-\frac{r^2}{a^2})^n \cdot 2\pi r dr. \tag{2}$$

Finally, the equation for the tangential stress distribution between the single-grain diamond and rock is as follows:

$$F_t = \int_0^a \tau_0(1-\frac{r^2}{a^2})^{1/2} \cdot 2\pi r dr \tag{3}$$

where τ_0 is the shear force at the center of circle.

The theory of the finite element method has also been introduced [29]. Let the spatial domain occupied by the contact system at moment t be Ω. The exposure problem can then be formulated as:

$$\int_{\Omega} \sigma \delta \varepsilon d\Omega - \int_{\Omega} F_V \delta u d\Omega - \int_{\Gamma_f} q_u \delta \varepsilon dS - \int_{\Gamma_c} q_\varepsilon \delta u dS + \int_{\Omega} \rho a \delta u d\Omega = 0 \quad (4)$$

where F_V denotes the body force, q_u and q_ε denote the boundary stresses, σ denotes Cauchy's stress, Γ_f denotes the boundary of the given boundary stress, Γ_c denotes the contacting boundary, $\delta\varepsilon$ denotes the virtual strain, δu denotes the virtual displacement, ρ denotes the density, and a denotes the acceleration. The spatial domain Ω is discretized by the finite element method. We introduce the virtual displacement field, and the equation is as follows:

$$m\ddot{u} = p(t) + c(u, \alpha) - f(u, \beta) \quad (5)$$

where m is the mass matrix, $\ddot{u}$ is the acceleration vector, t is a time variable, p is the external force vector, c is the contact force and friction vector, f is the internal stress vector, u is the object displacement, α is a variable associated with the contact surface characteristics, and β is a variable associated with the constitutive relation of the materials.

2.2 Drill bit -rock interaction model

As illustrated in Fig. 3, this section introduces the interaction model between the impregnant diamond bit and the rock and compares the torque of CB with DB.

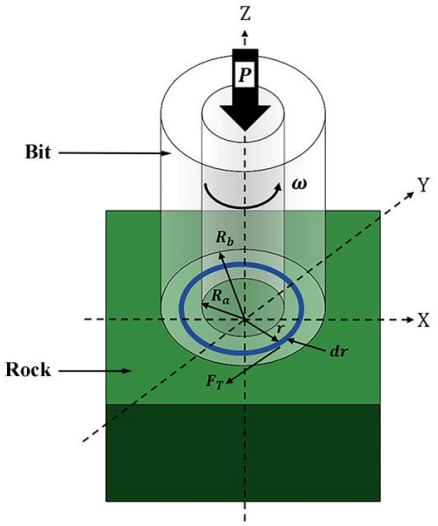

Fig. 3. Drill bit-rock interaction model

The reactive torque of the impregnated diamond bit during drilling was mainly due to the reaction force when cutting the rock with diamond particles and the friction force of the matrix.

Because the diamond particles exposed at the bottom of the bit are small, numerous, and messy in distribution, it is not possible to analyze and sum the forces on all particles. To facilitate the calculation, we treated the bottom surface of the drill bit as a flat circle, without affecting the comparison results. Then, the torque applied to the bit can be represented as:

$$M = \int_{R_a}^{R_b} 2\pi k F_T l^2 dl = \frac{3}{4}\pi n F_T ({R_b}^3 - {R_a}^3) \quad (6)$$

where k is the number of diamond particles per element area on the bottom surface of the bit, F_T is the force per element area consumed in rock breaking and friction, l is the radius of the integral micro-element, R_a、R_b are the inner and outer diameters of the bit, respectively.

Based on the structural characteristics of CB and DB, we assumed that the inner diameter of the CB was R_1 and the outer diameter was R_4, the inner diameter of the IB was R_1 and the outer diameter was R_2, and the inner diameter of the OB was R_3 and the outer diameter was R_4. The direction of rotation of the CB was

defined as positive. OB rotates in the same direction as CB, whereas IB rotates in the opposite direction. Then, the reactive torque of the CB is calculated by

$$M_s = -\frac{3}{4}\pi k F_T ({R_4}^3 - {R_1}^3) \tag{7}$$

Similarly, we obtained the counter torque M_o applied to OB and the counter torque M_i applied to IB.

$$M_i = \frac{3}{4}\pi k F_T ({R_2}^3 - {R_1}^3) \tag{8}$$

$$M_o = -\frac{3}{4}\pi k F_T ({R_4}^3 - {R_3}^3) \tag{9}$$

Then, the combined torque on the DB can be calculated as:

$$M_d = -\frac{3}{4}\pi k F_T \left[\left({R_4}^3 - {R_3}^3\right) - \left({R_2}^3 - {R_1}^3\right)\right] \tag{10}$$

From these, we theoretically concluded that the counter torque of the DB during drilling is much lower than that of the CB. Ideally, Equation 11 is satisfied, and there is no fluctuation during drilling when DB can even achieve "*no counter torque*" drilling. This provides a theoretical reference for DB design size.

$${R_4}^3 - {R_3}^3 = {R_2}^3 - {R_1}^3 \tag{11}$$

2.3 Rock constitutive relations and failure criterion

Rock is an anisotropic and nonlinear material that undergoes elastic deformation, plastic deformation, and brittle fracture under force. A suitable strength theory is particularly pivotal for rock-breaking simulations. In this study, the rock failure criterion was established based on the Drucker-Prager (D-P) criterion, which is an extension and generalization of the Mohr-Coulomb and well-known Mises criteria in plastic mechanics. The D-P criterion considers not only the effect of intermediate principal stress but also shear-induced expansion [30]. Therefore, the D-P criterion is widely used to study the rock-crushing process, and its expression is as follows:

$$\alpha I_1 + \sqrt{J_2} - K = 0 \tag{12}$$

$$I_1 = \sigma_1 + \sigma_2 + \sigma_3 \tag{13}$$

$$J_2 = \frac{1}{6}[(\sigma_1 - \sigma_2)^2 + (\sigma_2 - \sigma_3)^2 + (\sigma_3 - \sigma_1)^2] \tag{14}$$

where I_1 is the first invariant of the effective stress tensor, J_2 is the second invariant of the stress deviator tensor, and σ_1, σ_2 and σ_3 are the principal stresses of the effective stress. The experimental constants related only to the friction angle φ and cohesion c of rocks are α and K, respectively, and the equation is as follows:

$$\alpha = \frac{2\sin\varphi}{\sqrt{3}(3-\sin\varphi)} \tag{15}$$

$$K = \frac{6c\cos\varphi}{\sqrt{3}(3-\sin\varphi)} \tag{16}$$

Plastic strain occurs when the rock is pressed into and sheared by diamond particles. When the equivalent plastic strain value of the rock elemental node reaches its limit, the material starts to get damaged. The judgment criterion can be expressed as follows:

$$\bar{\varepsilon}^{pl} \le \bar{\varepsilon}_f^{pl} \tag{17}$$

where $\bar{\varepsilon}^{pl}$ is the equivalent plastic strain of the rock element, $\bar{\varepsilon}_f^{pl}$ is the equivalent plastic strain of the failure element.

3 Finite element analysis of rock breaking process

3.1 Basic assumptions

This study focuses on the rock-breaking process of the DB, which is compared with CB. To facilitate the establishment and solution of the bit and rock model, the simulation model is reasonably simplified based on the research emphasis. (1) Because the hardness and strength of diamond particles are much greater than those of rocks, and the stress distribution of the bit is not essential in this study, it is assumed that the bit is a rigid body. (2) The bit and rock are homogeneous continuous media, and the influence of the porous medium is neglected. (3) Rock elements were removed immediately after failure, neglecting the influence of repeated fragmentation on continuous drilling. (4) The influence of the flow and temperature fields on the rock-breaking process was not considered.

3.2 Geometric model and material properties

The numerical program ABAQUS was used to study the rock crushing process and simulate the evolution of the damage initiation and propagation. Nonlinear dynamical finite element models, including the CB-rock and DB-rock systems, were developed. As illustrated in Fig. 4, the cutaway views of the two models were selected for ease of observation. The purpose of the pressure sheet was to ensure that the weight of the DB was the same as that of the CB. To unify the dimensions of the two bits, the IB had the same inner diameter as the CB and the OB had the same outer diameter as the CB. As for the drilling parameters, the direction of the rotation speed of the IB and OB were opposite, the sizes of which were the same as those of the CB. The weights applied to the CB and DB were identical. The sizes and drilling parameters of the bits are listed in Table 1. It is worth noting that when designing IB and OB, in order to theoretically balance the reactive torque, the dimensions of IB and OB satisfied equation 11.

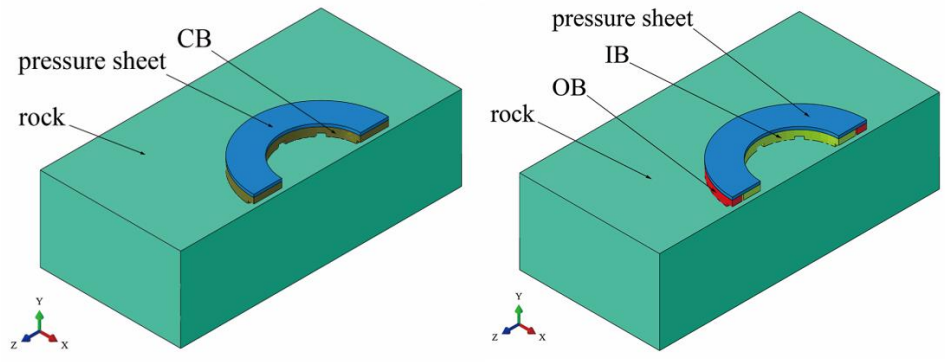

(a) (b).

Fig. 4. (a) Cutaway view of the CB and rock model. (b) Cutaway view of the DB and rock model.

Table 1 The bit sizes and drilling parameters

Bit type	Inner diameter (mm)	Outer diameter (mm)	Rotary speed (rpm)	Weight on bit (N)
CB	28	48	300	1000
IB	28	40	-300	Total 1000
OB	41	48	300	

It is known that the computation time of a program increases geometrically with the grid encryption. Because of the small size and large number of diamond particles on the bit, a very fine grid is required if the model is built according to the actual size of the diamond, which affects the calculation accuracy [31]. After repeated simulation tests, a model size and mesh division form suitable for the calculation of the diamond particles were established. As shown in Fig. 5, the diameter of one diamond particle was set to 1 mm and the spacing was 0.5 mm. Diamond particles were uniformly distributed on the bottom of the bits and the exposed height was uniform at 0.5 mm, without considering the shedding of diamond particles and the self-sharpening of the bits.

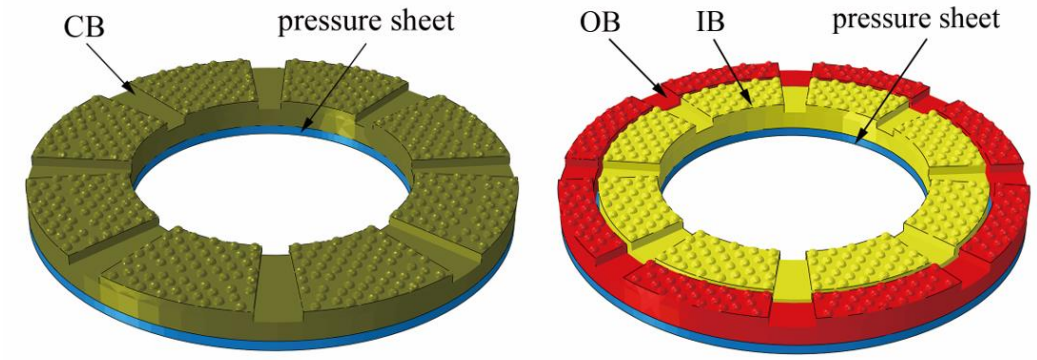

(a) (b).

Fig. 5. (a) Model of CB and pressure sheet. (b) Model of DB and pressure sheet.

To control for irrelevant variables, the same mesh density and partitioning were used for both the finite element models of the CB-rock and DB-rock systems. As illustrated in Fig. 6, both the rock and pressure sheet were discretized using eight-node linear hexahedral reduced integration elements, among which hourglass control was considered (C3D8R). The bits were all discrete with tetrahedral elements (C3D4), which were locally encrypted in the cutting area to improve calculation efficiency. During the simulation, the lower surface and sides of the rock were set with fixed constraints to limit its movement completely. The translation and rotation of the bit were limited in the X and Z directions. WOB was applied to the pressure sheet in the same direction as the bit drilling direction. The contact between the surface of the bit and the rock element was face-to-face with a friction coefficient of 0.3. This numerical model adopts an international system of elements (mm-N-s). The basic parameters for each part of the material are listed in Table 2. Because the stress distribution of the bit was not analyzed in this study, the overall material of the bit was set to diamond to simplify the calculation. A pressure sheet was used to simulate the pressure of the drill pipe, and the material was steel. Granite was used as the rock material.

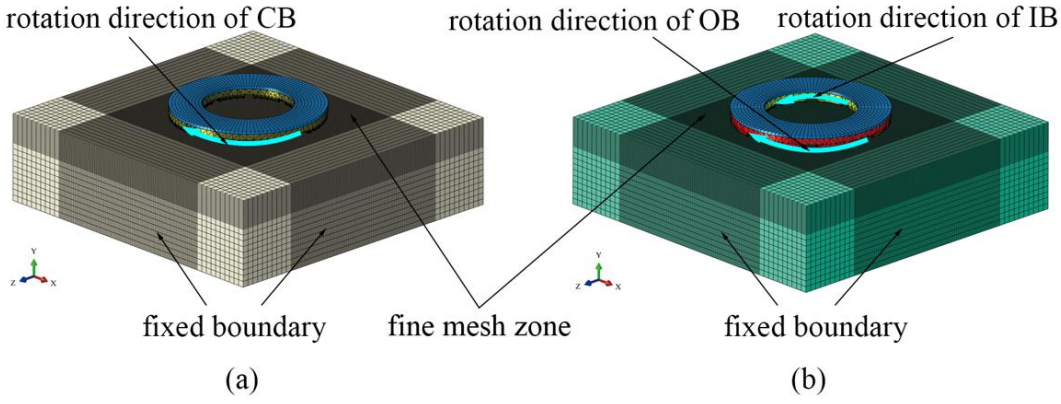

Fig. 6. Mesh and boundary conditions: (a) the CB-rock system; (b) the DB-rock system.

Table 2 The physical parameters for finite element analysis

Model	Material	Density ($kg \cdot m^{-3}$)	Elastic modulus (Gpa)	Poisson's ratio
Bit	Diamond	3510	897	0.07
Pressure sheet	Steel	7890	209	0.269
Rock	Granite	2700	48.4	0.25

3.3 Calibration of rock model parameters

This section focuses on the verification and calibration of rock parameters for the reliability of the simulation results. The uniaxial compression simulation of the granite model using the finite element software ABAQUS was compared with the experimental results. To minimize the error caused by the experimental samples, a granite sample of Ø50×100 mm was drilled and the surface was polished. The rock model used for the numerical simulation was the same size as that of the experimental sample. The rock material parameters are presented in Table 2. Additionally, a coaxial rigid disk was added to the upper surface of the model. A completely fixed constraint was applied to the bottom surface, and a compressive displacement load of 5 mm was applied to the disk, which only had z-directional degrees of freedom. Fig. 7 shows the failure patterns of the rock under uniaxial compression. The simulated result of uniaxial compression was very similar to the experimental results in terms of morphology. They consistently exhibited a V-shaped fracture pattern (red dashed lines in Fig. 7 are fractures), which is related to the internal friction angle of the rock. The experimental test results (red curve) and numerical simulation results (blue curve) for the uniaxial compression of granite under the same parameter conditions are shown in Fig. 8. The peak intensity and slope of the elastic segment of the two stress-strain curves were consistent, and both exhibited brittle damage after the peak. This study considers that this model is reliable for simulating the fracturing and stress-strain behavior of rocks.

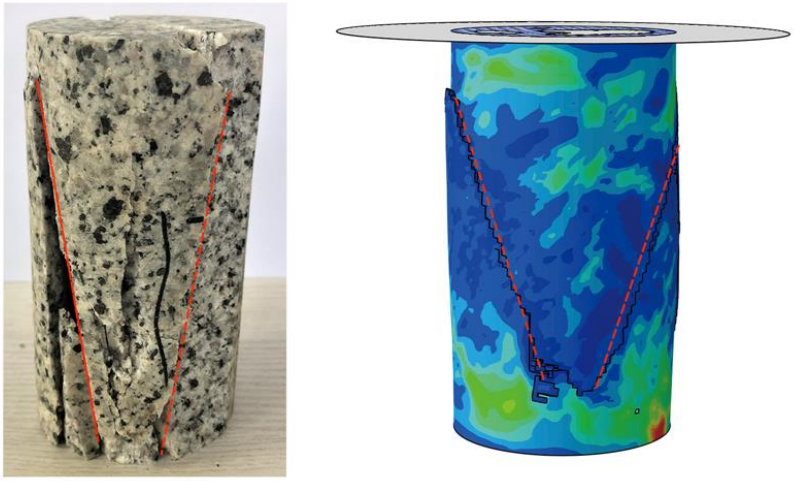

(a) (b)

Fig. 7. Comparison diagram of rock failure: (a) laboratory test; (b) numerical simulation.

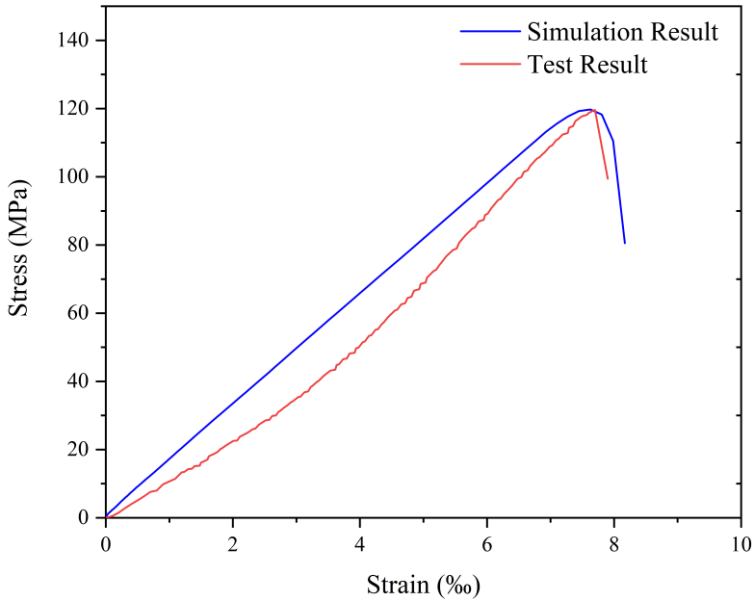

Fig. 8. Stress-strain curves obtained from numerical simulations and laboratory experiments.

4 Simulation results and discussion

4.1 Analysis of rock breaking mechanism

To compare the differences in the rock-breaking mechanism between DB and CB, this section compares the rock-breaking morphology, cutting force of the bit, and mechanical specific energy (MSE).

Fig. 9 compares the equivalent plastic strain of the rock at 0.03, 0.06, 0.12, and 0.15 s. At 0.03 s, the bits were in contact with the rock surface under pressure and the compressive stress dominated. As the bottom surfaces of the CB and DB were equal, there was little difference in the plastic strain of the rock. At 0.06 s, the crater formed by the DB was significantly larger than that of the CB, and the DB formed a shear damage zone at the junction of the IB and OB, while the CB did not exhibit this phenomenon. At 0.12 s, the breaking area of the rock under the action of the DB was the first to form a closed loop, and both types of rocks were broken by the outer ring first, which could be due to the fact that the linear velocity of the outer ring of the bit is larger than that of the inner ring. At 0.15 s, the DB took the lead to break the first layer of rock elements and formed a cylindrical core, while the CB did not break the first layer. Therefore, the efficiency of DB breaking rock was higher than that of CB breaking rock.

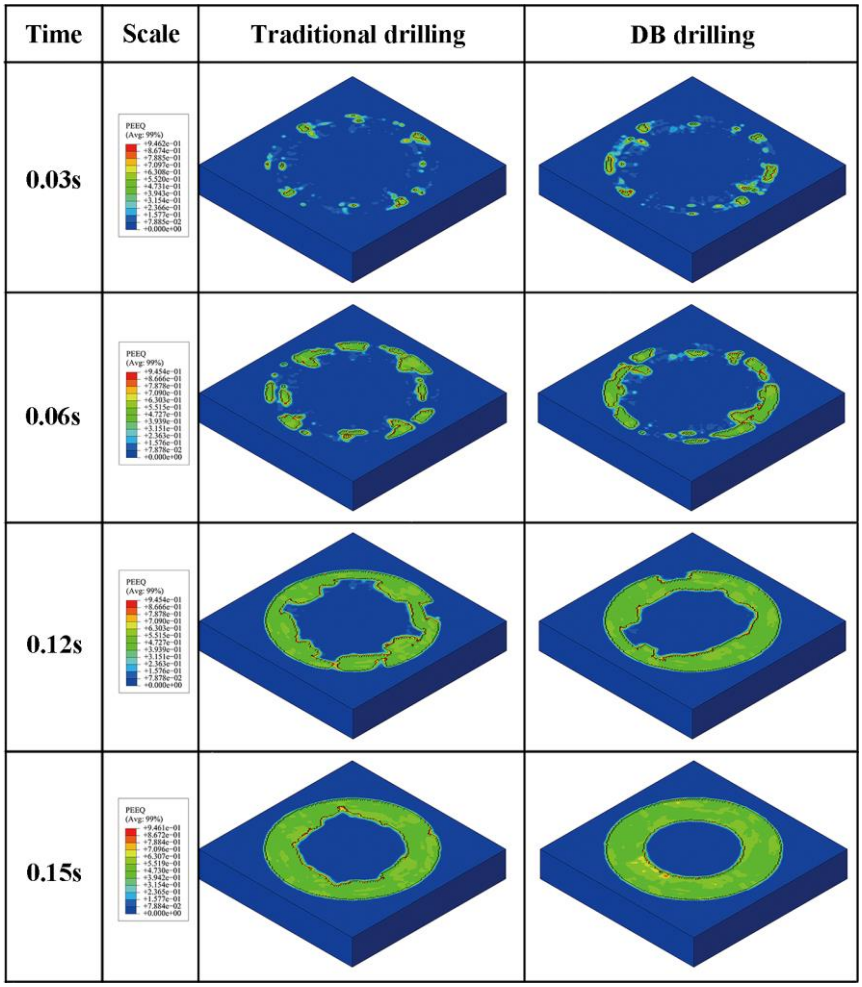

Fig. 9. Comparison of rock equivalent plastic strain.

To further illustrate the shear-breaking effect of DB on the rock in the junction breaking zone, as shown in Fig. 10, the maximum principal stress of the rock (0.06s) was selected in this study. It can be seen that the maximum principal stress on the rock during DB drilling was 12.4% higher than that during CB drilling. We then used four areas to illustrate the breaking effect of the rock surface under the action of DB. Under the grinding action of the diamond particles, scratches first appeared on the rock surface, as shown in Region 3. Subsequently, the scratches gradually formed small pits, as shown in Region 2. Some rock ridges formed between the breaking pits, and these rock elements were subjected to tensile stress. This indicates that DB had a shear-breaking effect on the rock. Subsequently, some of the small crushing pits merged to form large crushing pits, as shown in Region 1. At this point, the rock elements between the large fracture pits were already relatively fragile and could easily form volumetric fractures, as shown in Region 4.

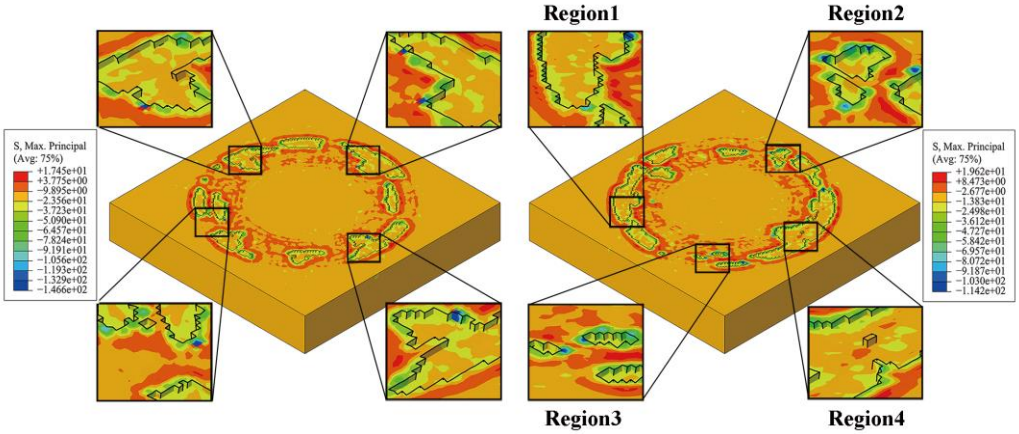

(a) and (b).

Fig. 10. Comparison of Max. principal stress: (a) rock drilled by CB; (b) rock drilled by DB.

Rock breaking is the process of alternating the action of macro-and microcrushing forms. During the rotary cutting process, small and large chips are formed and flow out continuously, and the cutting force of the drill bit varies continuously. The investigation of the variation law of the cutting force is beneficial for the analysis of the rock-breaking mechanism. The results in Fig. 11 clearly indicate that periodic fluctuations in the tangential force occurred with time. In addition, the force increased and then decreased in each cycle, indicating that the grinding process of the impregnated diamond bits also resulted in stress accumulation and release. The tangential forces and fluctuations of IB and OB were significantly smaller than those of CB. Compared with the CB, the average tangential force of the IB decreased by 18.8% and that of the OB decreased by 35.8%. Therefore, DB provides a more consistent cutting performance, which contributes to more efficient drilling.

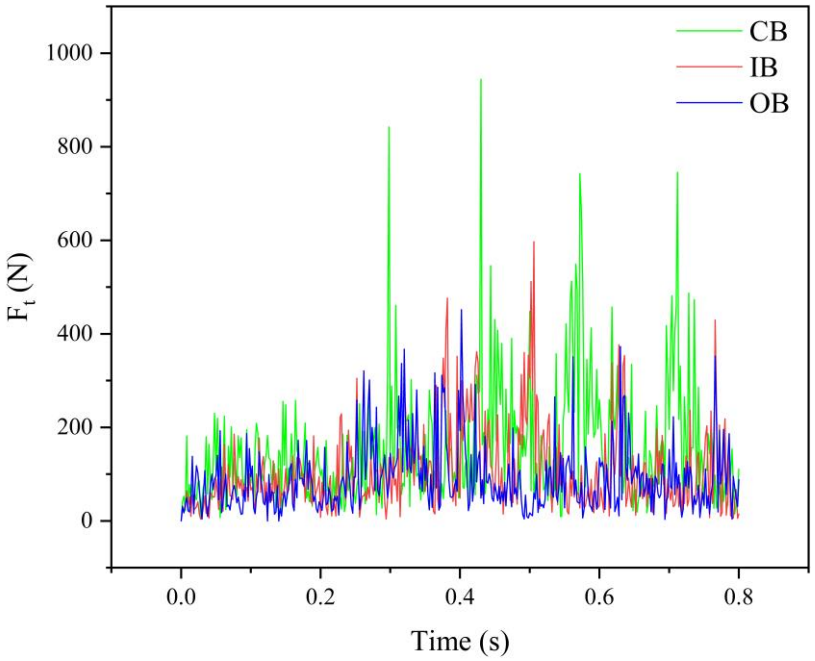

Fig. 11. Relationship between the tangential force and time.

4.2 Damage analysis of wellbore and core

The damage to the wellbore and core can be used to analyze the effect of DB drilling to reduce disturbance. Fig. 12 shows the cross-sectional stress of the rock during rock breaking with the CB and DB. To facilitate a comparative observation, the von Mises stress diagram of both was set to the same scale. In this study, four time points were selected for description. At 0.2 s, the rock fragmentation pit was shallow and no core or wellbore was formed, at which time the forces on the rock were similar between the CB and DB. At 0.49 s, the CB started to produce weak stress in the middle of the core, but the DB did not exhibit this phenomenon. At 0.6 s, the CB produced significant disturbance to the core, while the DB had no stress effect on both the core and wellbore. At 0.8 s, the CB started to disturb the surrounding formation, but the DB only weakly disturbed the core at this time. Therefore, it can be concluded that the disturbance to the core and formation during DB drilling is significantly less than that of CB drilling under the same conditions, and DB can achieve the purpose of micro-disturbance drilling. To further analyze the damage of the two types of bits on the rock at different locations, seven rock elements were selected. As shown in Fig. 13, they were all 1.2 mm from the rock surface. E1 is the core element immediately adjacent to the core wall, E2 is the core wall element, E3 is the element in

the IB breaking zone, E4 is the element in the junction breaking zone, E5 is the element in the OB breaking zone, E6 is the wellbore element, and E7 is the formation element immediately adjacent to the wellbore.

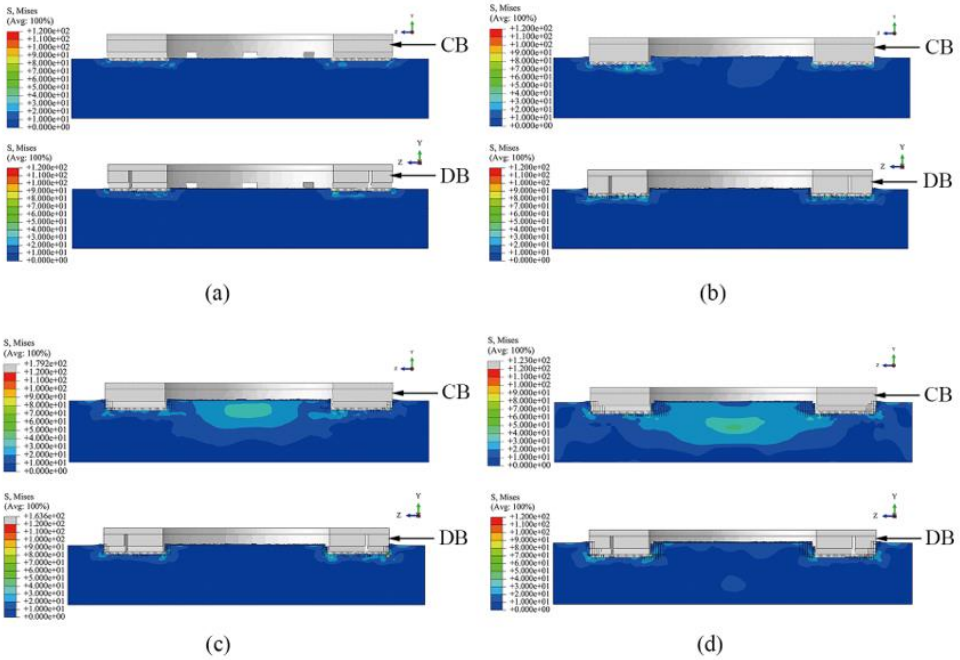

Fig. 12. Comparison of Mises stress distribution in rock profiles: (a) 0.2 s; (b) 0.49 s; (c) 0.6 s; (d) 0.8 s.

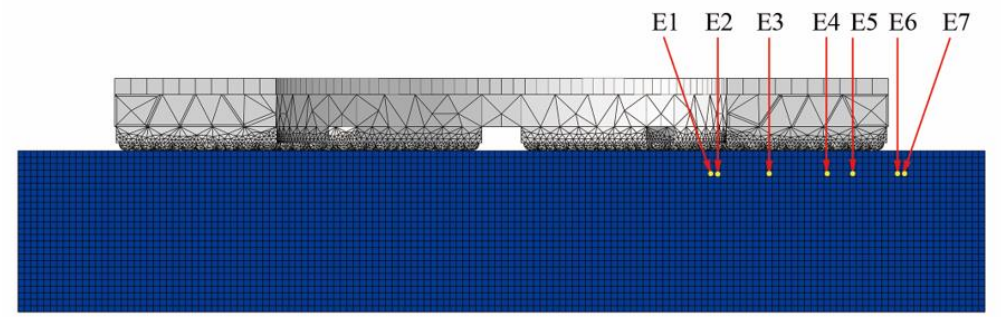

Fig. 13. Selection of rock elements.

Fig. 14 shows the damage of the core and wellbore elements. After the simulation, the damage to the core element (E1) under the DB drilling conditions was reduced from 0.072 to 0.057, a 20.8% reduction compared to the CB drilling. Similarly, the damage to the core wall element (E2) was reduced from 0.222 to 0.208, a 6.3% reduction. The damage to the wellbore element (E6) was reduced from 0.333 to 0.219, a 34.2% reduction. The damage to the formation element (E7) decreased from 0.071 to 0.045, a reduction of 36.6%. Fig. 15 shows the comparison of rock elements in the breaking zone under the two drilling conditions. For these elements to be broken into holes, including the elements in the breaking zone of the IB (E3), the breaking zone of the junction (E4), and the breaking zone of the OB (E5), the DB could complete the breaking in preference to that by CB, with 27.8%, 16.8%, and 15.6% improvement in efficiency, respectively. After comparing the damages to the seven elements, we concluded that the DB not only disturbs the formation and core significantly less than the CB, but also breaks the rock more efficiently than CB.

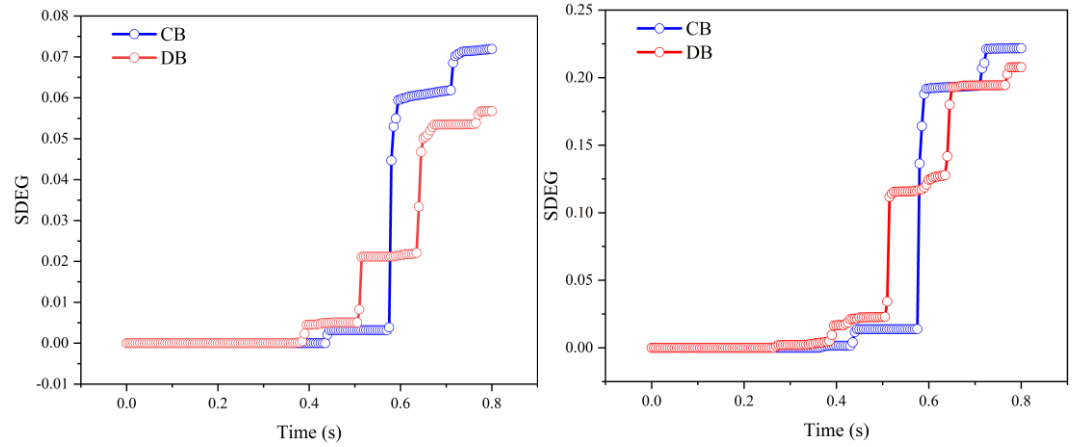

(a) SDEG of E1 (b) SDEG of E2

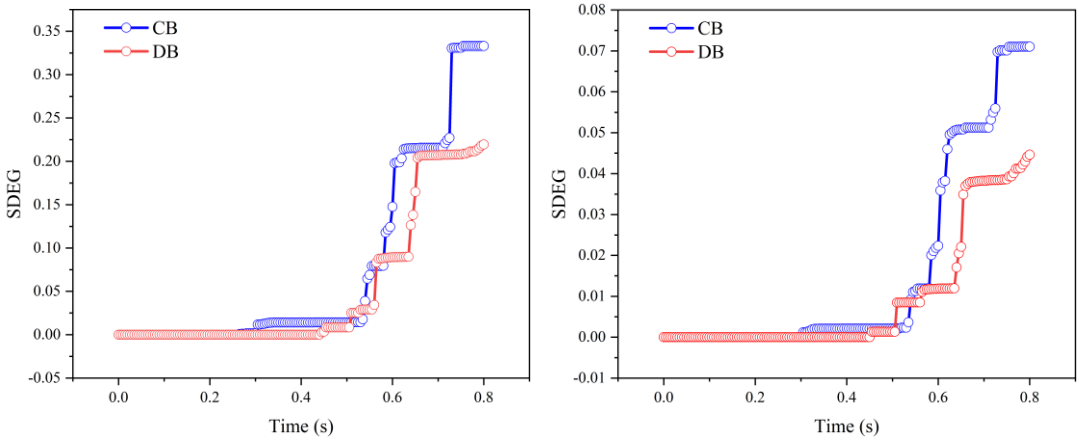

(c) SDEG of E6 (d) SDEG of E7

Fig. 14. SDEG of the core and wellbore elements in rock.

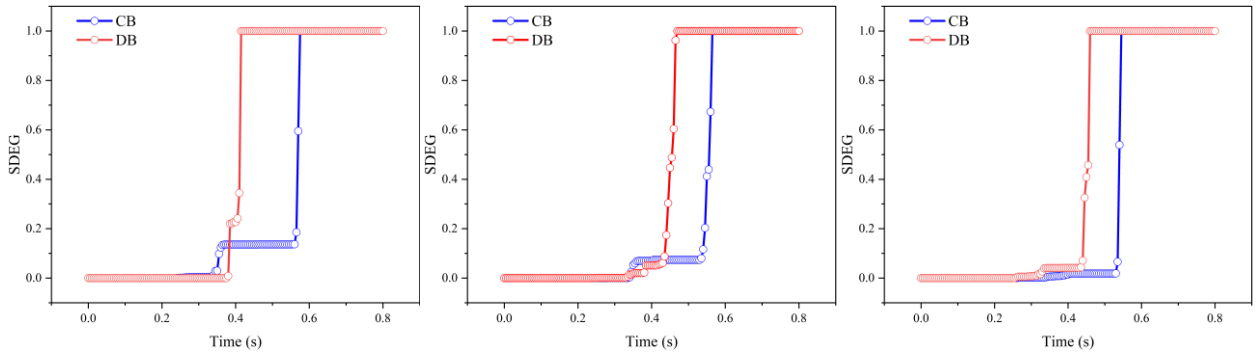

(a) SDEG of E3, (b) SDEG of E4, (c) SDEG of E5

Fig. 15. SDEG of the breaking zone elements in rock: (a) E3; (b) E4; (c) E5.

4.3 Comparison of the drill bit movement

According to the working principle of *Downhole Drilling Tool System of Torque Self-balancing*, the reactive torques of IB and OB can cancel each other. Fig. 16a shows the variation in the reactive torque on IB and OB with time during the DB drilling process. The rotation direction of OB is defined as the positive direction, and that of IB is defined as the negative direction. It can be seen that the reactive torque fluctuates periodically with time, which is due to the granite being a brittle material. Before breaking the rock, the bit must accumulate energy, at which time the reactive torque gradually increases. After breaking the rock, there is a stage of sudden release of stress when the reactive torque of the rock on the bit decreases suddenly. The bit regains contact

with the unbroken rock when it builds up energy. The average value of the reactive torque of the rock to the IB was -6.0 $N \cdot m$, while the OB was 6.1 $N \cdot m$. Despite certain fluctuations, the IB and the OB could still achieve a balance of reactive torque. To further compare the difference in reactive torque between DB and CB, the vector sum of the IB and OB reactive torques at each time point was taken as the reactive torque of DB and compared with that of CB. The results are shown in Fig. 16b, where the average magnitude and fluctuation range of the reactive torque of the DB are significantly smaller than those of the CB. It can be illustrated that DB weakens the reactive torque of the rock on the drilling tool during the drilling process, specifically reducing it by 69.7%.

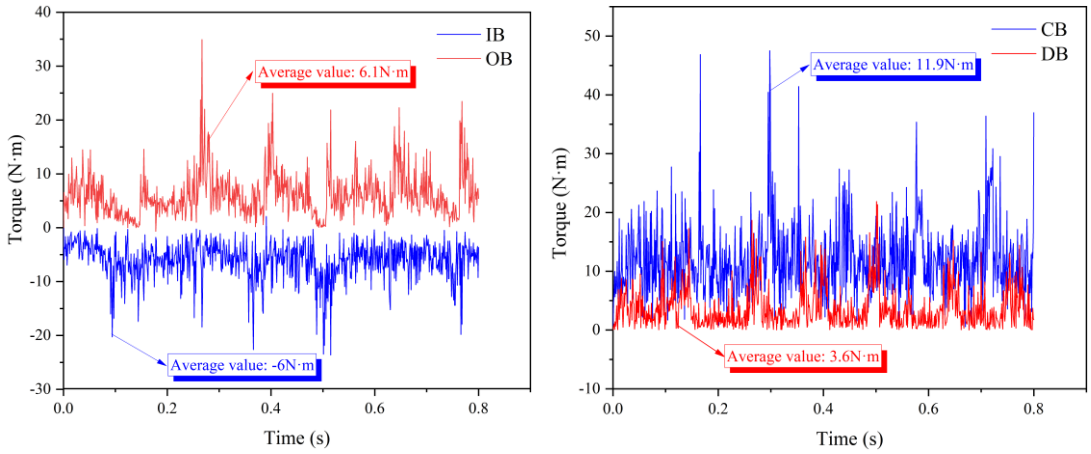

(a) (b)

Fig. 16. Comparison of the reactive torque on bit: (a) IB and OB; (b) CB and DB.

The MSE was used to specifically quantify the drilling efficiency enhanced by DB [32]. MSE refers to the energy consumed by the crushing unit volume of rock and is an important indicator for evaluating the drilling and tool breaking efficiencies. In other words, the lower the rock-breaking ratio, the higher the rock-breaking efficiency [33]. The MSE can be expressed as follows:

$$MSE = \frac{N}{S} + \frac{120\pi \cdot T \cdot \omega}{v \cdot S} \tag{18}$$

where MSE is the mechanical specific energy, N is the weight on bits, T is the torque of the bit, ω is the bit rotation speed, S is the bit area, v is the rate of penetration.

As CB and DB have the same diamond particle distribution and WOB, and the impregnated diamond drill bit grinds the rock mainly, the MSE is mainly contributed by the torque. This study ignored the effect of the axial force and considered only the energy consumption of the tangential force. As shown in Fig.17, the MSE of DB was reduced by 55.7% and the ROP was increased by 13.8% compared to that of CB. This confirms our assumption in Section 4.1 that DB has a higher drilling efficiency owing to its more stable rock-breaking process.

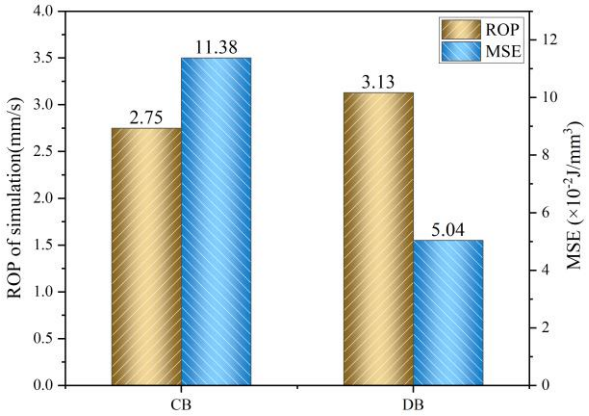

Fig. 17. Comparison of ROP and MSE between CB and DB

5 Experimental verifications

Relying on *Downhole Drilling Tool System of Torque Self-balancing*, a drilling comparison experiment was conducted between DB and CB. Fig. 18 illustrates a schematic of the entire system used to perform the laboratory drilling experiment. It contains five parts: drilling rig, DB, tank, air compressor, and automatic control system. To ensure the same conditions for the experiment and simulation, CB and DB of the same size as the simulation were prepared. The experimental bit size and drilling parameters were identical to those used in the simulation.

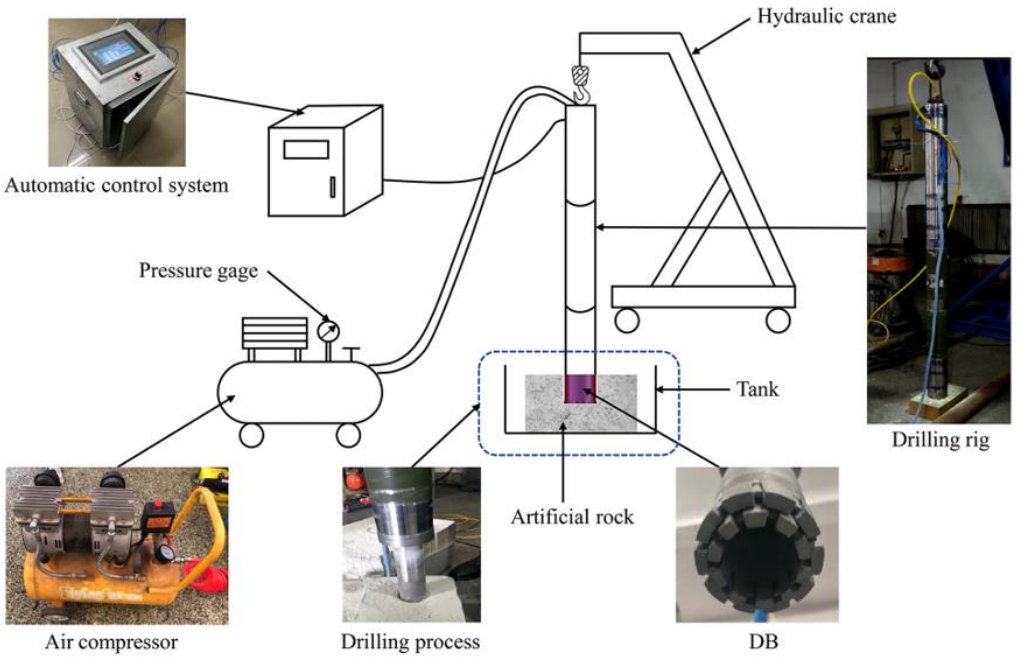

Fig. 18. Schematic and photography of the drilling experimental setup

The experimental granite was the same as the granite material used to calibrate the model parameters presented in Section 3.3. Core drilling experiments were conducted on the CB and DB under the same drilling conditions. The experimental results are as follows: (1) Fig. 19 shows the drilling hole comparison of granite drilled by CB and DB. Borehole-1 was drilled by the CB, and borehole-2 by the DB. Volume breakage occurred at the junction of the IB and OB at the bottom of the hole, while the bottom of borehole-2 was quite flat. DB has a shear breaking effect and facilitated the breaking of rocks, as described in Section 4.1. (2) The core and wellbore wall diameters were considered as drilling damage indicators. DB drilling could reduce damage to the core and wellbore wall by 24.7% and 33.3%, respectively, as compared to those with the CB drilling. This result is in better agreement with the simulation results in Section 4.2, which verifies the effect of DB in reducing the drilling disturbance. (3) Three sets of drilling experiments were conducted to compare the ROP of the CB with that of the DB, as shown in Fig. 20. DB increased the ROP by 16.3%, 13.7%, and 14.5% in the three sets of experiments with an average improvement of 14.8%. The results of this drilling comparison experiment were in good agreement with the simulation results, thereby verifying the accuracy of the finite element model simulation analysis.

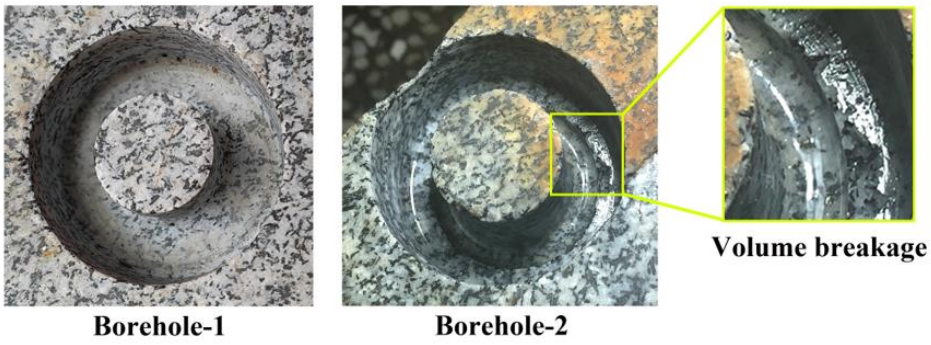

Fig. 19. Drilling hole comparison of granite drilled by the CB and the DB.

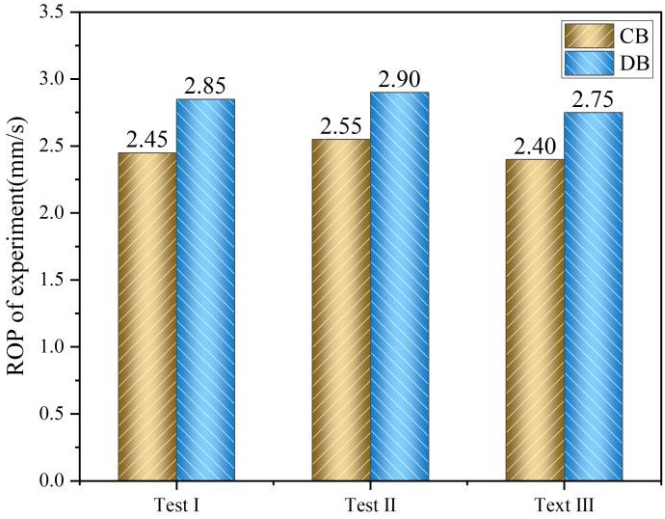

Fig. 20. Comparison of ROP between the CB and DB drilling.

In addition, we conducted a comparative drilling experiment on a looser artificial conglomerate, and the results are shown in Fig. 21. The integrity of borecore-4 drilled using the DB was much greater than that of core-3 drilled using the CB. It can be clearly seen that the disturbance to the wellbore wall and core during drilling was reduced by the DB compared with the CB. The CB always disturbs the core and wellbore wall as the drilling depth increases, resulting in severe core damage and roughness of the wellbore wall. While DB only caused some disturbance to the core at the open hole, stable coring work was quickly achieved, and the sidewall surfaces of both the core and wellbore wall were very smooth. As shown in Fig. 18, the rock does not need to be fixed during DB drilling, and the upper drilling rig is largely free from reactive torque. In this experiment, the core recovery percentage of the CB was 34.1%, and that of the DB was 83.3%, which was an improvement of 55.2%. This indicates that the ability to reduce drilling disturbance is more pronounced when drilling into softer, looser rocks with DB than into hard rocks such as granite.

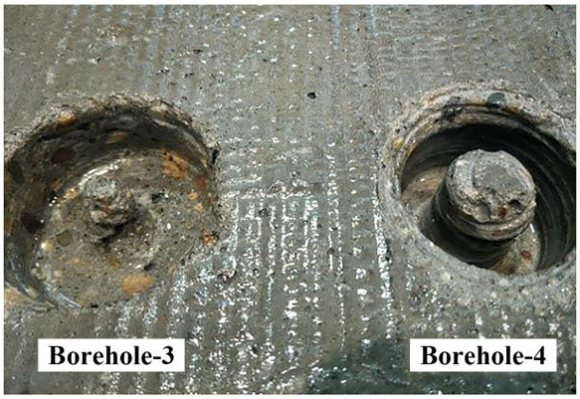

Fig. 21. Drilling hole comparison of conglomerate drilled by the CB and the DB

6 Conclusions

In this study, it was verified through calculations that DB drilling technology reduced the stick-slip vibration and disturbance to the core and formation. Subsequently, a nonlinear dynamical simulation was conducted to reveal the rock-breaking process, wellbore and core disturbance, and bit motion, which explained the differences in the rock-breaking mechanism between DB and CB. Finally, the simulation results were validated using a drilling experiment. The following conclusions were drawn:

(1) The theoretical calculation of the DB's reactive torque shows that DB can achieve "no reactive torque" drilling ideally when the cubic difference between the inner and outer radius of OB and IB is equal. This conclusion was verified using numerical simulation, where the average value of the reactive torque of the rock to the IB was -6.0 $N \cdot m$ and to the OB was 6.1 $N \cdot m$. This provides a theoretical suggestion for the size design of the DB.

(2) The simulation results show that DB forms a shear damage zone on rock at the junction of IB and OB compared with CB, which facilitates rock breaking and improves drilling efficiency. Specifically, the tangential force of IB decreased by 18.8%, whereas that of OB decreased by 35.8%. As a result, DB reduced the MSE by 55.7% and improved the ROP by 13.8%.

(3) The reactive torque generated by the DB was 69.7% lower than that generated by the CB. The disturbance to the formation and core was also less than that of the CB, specifically 20.8% less disturbance to the core and 36.6% less disturbance to the formation. This indicates that DB decreases the stick-slip vibration of the bit, which is beneficial for the core recovery and formation stability.

(4) The results of the drilling comparison experiment between DB and CB showed that the average ROP of DB self-balancing drilling increased by 14.8%. Damage to the core and wellbore wall was reduced by 24.7% and 33.3%, respectively. This is consistent with the numerical simulation results, thereby verifying our conclusions. During DB drilling, the ability to reduce drilling disturbance is more pronounced when drilling into softer, looser rocks.

Despite the above-mentioned advantages of DB drilling, this study only conducts a comparative study of impregnated diamond bits, and the rocks used for the numerical simulation were homogeneous rocks, which have certain limitations. In future research, it will be necessary to study the rock-breaking process of other types of dual drill bits, such as PDC bits, to further improve the theory of DB drilling.

Credit authorship contribution statement

Cong Zhang: Methodology, Software, Formal analysis, and Writing of the original draft. **Ke Gao:** Conceptualization, Funding acquisition, and Writing – review and editing. **Yan zhao:** Writing – review and editing, Data curation, Supervision. **Xiaobo Xie:** Investigation, Supervision. **Congshan Zhang**: Software, Data curation. **Xiaoshu Lv:** Software.

Declaration of competing interest

The authors declare that they have no known competing financial interests or personal relationships that could have influenced the work reported in this study.

Acknowledgments

This research was funded by the National Natural Science Foundation of China (Grant Nos. 42172345

and 41972324) and Scientific Foundation of the Education Department of Jilin Province (Grant No. JJKH20221016KJ and JJKH20221014KJ).

References

1. Howarth, D. F., & Rowlands, J. C.: Quantitative assessment of rock texture and correlation with drillability and strength properties. Rock Mech. Rock Eng. **20**, 57-85 (1987)
2. Liu, W., Zhou, Y.C.: Prospective Study on Managed Pressure Drilling Technology of an Ultra-Deep Complex Well. Acta Geol. Sin. - Engl. Ed. **93**, 334–334 (2019). https://doi.org/10.1111/1755-6724.14121
3. Dong, G.J., Chen, P.: A Review of the Evaluation, Control, and Application Technologies for Drill String Vibrations and Shocks in Oil and Gas Well. Shock Vib. **2016**, 1–34 (2016). https://doi.org/10.1155/2016/7418635
4. Xu, X.X., Gu, H.R., Kan, Z.T., Zhang Y.Z., Cheng J.L., Li Z.Y.: Properties of Drillstring Vibration Absorber for Rotary Drilling Rig. Arab J Sci Eng. **45**, 5849–5858 (2020). https://doi.org/10.1007/s13369-020-04562-y
5. Huang, K.L., Yang, Y.X., Liu, Y., Niu, Q.Z.: Vibration failure and anti-vibration analysis of an annular-grooved PDC bit. Eng Fail Anal. **115**, 104658 (2020). https://doi.org/10.1016/j.engfailanal.2020.104658
6. Wang, W., Peng, J.M., Wang, H.Y., Chen, C., Wang, X.L., Fu, W.G.: FEM simulation analysis of sampling disturbance with PCS drill bit in gas-hydrate-bearing stratum. J. Cent. South Univ. **45**(4): 1183–1189 (2014).
7. Zhu, H.Y., Deng, J.G., Xie, Y.H., Huang, K.W., Zhao, J.Y., Yu, B.H.: Rock mechanics characteristic of complex formation and faster drilling techniques in Western South China Sea oilfields. Ocean Engineering. 44, 33–45 (2012). https://doi.org/10.1016/j.oceaneng.2012.01.031
8. Ledgerwood, L.W., Spencer, R.W., Matthews, O., Bomidi, J.A., Mendoza, J.A., Hanson, J.M.: The Effect of Bit Type on Reactive Torque and Consequent Tool-Face-Control Anomalies. SPE Drill. Complet. **31**, 095–105 (2016). https://doi.org/10.2118/174949-PA
9. Liu, Y.S., Gao, D.L.: A nonlinear dynamic model for characterizing downhole motions of drill-string in a deviated well. J. Nat Gas Sci. Eng. **38**, 466–474 (2017). https://doi.org/10.1016/j.jngse.2017.01.006
10. Ozaki, S., Hashiguchi, K.: Numerical analysis of stick-slip instability by a rate-dependent elastoplastic formulation for friction. Tribol. Int. **43**, 2120–2133 (2010). https://doi.org/10.1016/j.triboint.2010.06.007
11. Zhu, X.H., Tang, L.P., Yang, Q.M.: A Literature Review of Approaches for Stick-Slip Vibration Suppression in Oilwell Drillstring. Adv. Mech. Eng. **6**, 967952 (2014). https://doi.org/10.1155/2014/967952
12. Kyllingstad, A., Halsey, G.W.: A Study of Slip/Stick Motion of the Bit. SPE Drill. Eng. **5** (1988)
13. Besselink, B., van de Wouw, N., Nijmeijer, H.: A Semi-Analytical Study of Stick-Slip Oscillations in Drilling Systems. J. Comput. Nonlinear Dyn. **6**, 021006 (2011). https://doi.org/10.1115/1.4002386
14. Liu, X.B., Vlajic, N., Long, X.H., Meng, G., Balachandran, B.: Nonlinear motions of a flexible rotor with a drill bit: stick-slip and delay effects. Nonlinear Dyn. **72**, 61–77 (2013). https://doi.org/10.1007/s11071-012-0690-x
15. Zhu, X.H., Tang, L.P., Tong, H.: Effects of High-Frequency Torsional Impacts on Rock Drilling. Rock Mech. Rock Eng. **47**, 1345–1354 (2014). https://doi.org/10.1007/s00603-013-0461-0
16. Tian, K., Detournay, E.: Influence of PDC bit cutter layout on stick–slip vibrations of deep drilling systems. J. Petrol Sci. Eng. **206**, 109005 (2021). https://doi.org/10.1016/j.petrol.2021.109005
17. Gao, K., Zhang C., Zhao Y. et al: Theory and experiment of the dual-bit torque self-balancing drilling system for rescue drilling. Coal Geology & Exploration. **50**(11), 85−93 (2022). https://doi.org/10.12363/issn.1001-1986.22.06.0444

18. Gao, K., Sun, Y.H., Wang, Z.G. & Zhao, Y. et al.: Downhole drilling tool system of torque self-balancing [P]. US 10 724 300 B2 (2020).
19. Gao, K., Chen, H.K., Xu, X.H., Gao, H.T., Xie, X.B., Yan, L.P.: Rock fragmentation characteristics of double impregnated diamond bits with self-balancing reverse rotation. J. Jilin Univ. (Engineering and Technology Edition), **51**(3) (2021).
20. Zheng, M.Z., Li, S.J., Yao, Z., Zhang, A.D., Xu, D.P., Zhou, J.F.: Core discing characteristics and mitigation approach by a novel developed drill bit in deep rocks. J. Cent. South Univ. **27**, 2822–2833 (2020). https://doi.org/10.1007/s11771-020-4512-x
21. Rojek, J., Oñate, E., Labra, C., Kargl, H.: Discrete element simulation of rock cutting. International Journal of Rock Mechanics and Mining Sciences. **48**, 996–1010 (2011). https://doi.org/10.1016/j.ijrmms.2011.06.003
22. Dang, Y., Zhu, H., Yang, Z., Liu, Q.: Bionic Design and Numerical Simulation of Rough-Breaking Tool for Attapulgite Clay. Arab J Sci Eng. (2022). https://doi.org/10.1007/s13369-022-06999-9
23. Jaime, M.C., Zhou, Y., Lin, J.-S., Gamwo, I.K.: Finite element modeling of rock cutting and its fragmentation process. International Journal of Rock Mechanics and Mining Sciences. **80**, 137–146 (2015). https://doi.org/10.1016/j.ijrmms.2015.09.004
24. Yang, Y.X., Song, D.D., Ren, H.T., Huang, K.L., Zuo, L.: Study of a new impregnated diamond bit for drilling in complex, highly abrasive formation. J. Petrol Sci. Eng. **187**, 106831 (2020). https://doi.org/10.1016/j.petrol.2019.106831
25. Franca, L.F.P., Mostofi, M., Richard, T.: Interface laws for impregnated diamond tools for a given state of wear. Int. J. Rock Mech. Mining Sci. **73**, 184–193 (2015). https://doi.org/10.1016/j.ijrmms.2014.09.010
26. Ersoy, A., Atıcı, U.: Performance characteristics of circular diamond saws in cutting different types of rocks. Diamond and Related Materials. **13**, 22–37 (2004). https://doi.org/10.1016/j.diamond.2003.08.016
27. Popov V. L.: Contact Mechanics and Friction Physical Principles and Applications[M]. Springer Heidelberg, Berlin (2010)
28. Lindqvist, P.-A. Stress fields and subsurface crack propagation of single and multiple rock indentation and disc cutting. Rock Mech. Rock Eng. **17**, 97-112 (1984).
29. Zhong, Z.: Finite Procedures for Contact-Impact Problems[M]. Oxford University Press, Oxford (1993)
30. Liu, W.J., Qian, X.D., Li, T., Zhou, Y.L., Zhu, X.H.: Investigation of the tool-rock interaction using Drucker-Prager failure criterion. J. Petrol Sci. Eng. **173**, 269–278 (2019). https://doi.org/10.1016/j.petrol.2018.09.064
31. Yang, D.H.: Preliminary research of rock breaking methods and impregnated diamond core bit in scientific ultra-deep drilling process. Dissertation, China University of Geosciences, Wuhan (2012)
32. Teale, R.: The concept of specific energy in rock drilling. Int. J. Rock Mech. Mining Sci. **2**(2), 57-73 (1965)
33. Chen, X.Y., Fan, H.H., Guo, B.Y., Gao, D.L., Wei, H.S., Ye, Z.: Real-Time Prediction and Optimization of Drilling Performance Based on a New Mechanical Specific Energy Model. Arab J Sci Eng. 39, 8221–8231 (2014). https://doi.org/10.1007/s13369-014-1376-0